

## Research Article

# Autonomous Navigation of a Surveillance Robot in Harsh Outdoor Road Environments

Youjin Shin,<sup>1</sup> Donghyeon Kim,<sup>1</sup> Hyunsuk Lee,<sup>1</sup>  
Jooyoung Park,<sup>2</sup> and Woojin Chung<sup>1</sup>

<sup>1</sup> School of Mechanical Engineering, Korea University, Seoul, Republic of Korea

<sup>2</sup> Department of Control and Instrumentation, Korea University, Seoul, Republic of Korea

Correspondence should be addressed to Woojin Chung; smartrobot@korea.ac.kr

Received 11 April 2013; Revised 18 July 2013; Accepted 18 July 2013

Academic Editor: Yixiang Huang

Copyright © 2013 Youjin Shin et al. This is an open access article distributed under the Creative Commons Attribution License, which permits unrestricted use, distribution, and reproduction in any medium, provided the original work is properly cited.

This paper deals with the autonomous navigation problem of a mobile robot in outdoor road environments. The target application is surveillance in petroleum storage bases. Although there have been remarkable technological achievements recently in the area of outdoor navigation, robotic systems are still expensive due to a large number of high cost sensors. This paper proposes the reliable extraction algorithm of traversable regions using a single onboard Laser Range Finder (LRF) in outdoor road environments. The traversable regions are derived from the classifications of the road surfaces, curbs, and obstacles. The proposed scheme was experimentally tested in success. Since there are many potential applications that require autonomous service robots to move in semistructured road environments, the proposed scheme can be widely used as a low-cost practical solution.

## 1. Introduction

It is difficult to find reliable solutions for automated diagnosis of mechanical structures in harsh outdoor environment. Figure 1 is a petroleum base that is a typical example of harsh environment. It is common that a petroleum base is close to harbor in order to allow easy access to oil tankers. Maintenance by human operator is difficult because of the risk of explosion and huge workspace. Surveillance for security purpose is also required. Therefore, mobile robotic systems are advantageous. Direct access by a robot with leakage sensors and cameras is essential in practical applications.

The aim of this work is to provide a practical low-cost robotic surveillance solution in outdoor paved road environment. The road in a petroleum base is a restricted area without many dynamic obstacles. Therefore, environmental uncertainty is relatively low. However, a reliable day and night operation is required. The robot should be able to survive in various weather conditions.

Recently, the application area of mobile robots has been expanding [1–4]. Especially, outdoor navigation of mobile

robots has received much attention, fostering a large number of significant technological achievements [5, 6]. Typical examples are the automated robotic vehicles shown in DARPA challenge [7, 8]. Furthermore, some successful technologies can be found, for example, in [9, 10]. These technologies, however, are based on multiple high costs sensing equipment as solutions. Expensive sensing equipment is required to overcome a variety of uncertainties in unstructured outdoor environments. However, the high cost of these technologies limits the practical applications of robotic systems using these technologies.

This paper proposes a reliable extraction algorithm of traversable regions using a single onboard Laser Range Finder (LRF) in outdoor road environments. The traversable regions are derived from the classifications of the road surfaces, curbs, and obstacles.

Detection of road curbs or lanes has been studied. Vision systems are the common approach for road-lane detection. Wang's method [11], Vector Lane Concept [12], and Wu's method [13] are successful vision-based methodologies. However, the major drawback of vision systems is that



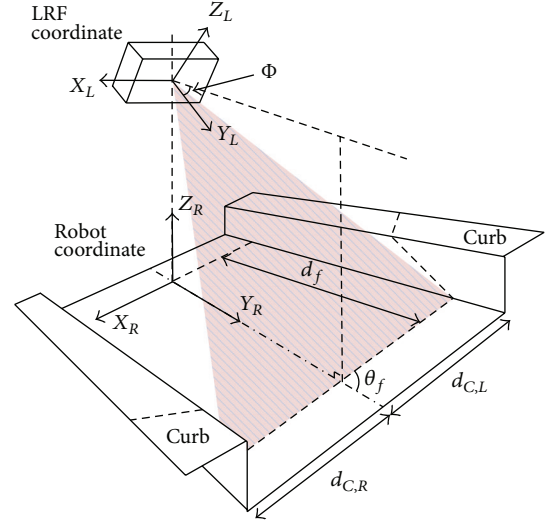
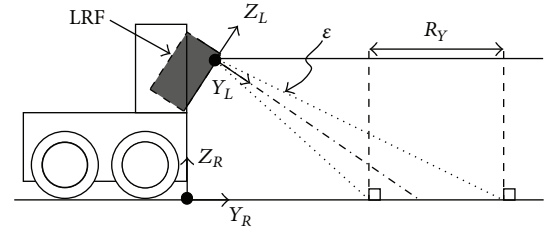
FIGURE 1: Target environment.

TABLE 1: Nomenclature.

Symbols	Meaning
$X_L, Y_L, Z_L$	LRF local coordinate
$X_R, Y_R, Z_R$	Robot local coordinate
$\Phi$	Nominal tilt angle of a LRF
$\varepsilon$	Tolerance of pitch angle
$\theta_f$	Angle between the detected road surface points and $Y_R$ -axis
$\theta_c$	Angle between the detected curb and $Y_R$ -axis
$d_f$	Horizontal distance from the LRF origin to the road surface points
$d_c$	Gap between two parallel curbs. Road width.
$d_{C,R}$	Lateral margin from the LRF origin to the right curb
$d_{C,L}$	Lateral margin from the LRF origin to the left curb
$X_{\text{pass}}$	Detected traversable region in $x$ direction
$Y_{\text{pass}}$	Detected traversable region in $y$ direction
$R_Y$	Expected $y$ range of the road surface points

they have difficulty when confronted with bad weather or illumination change.

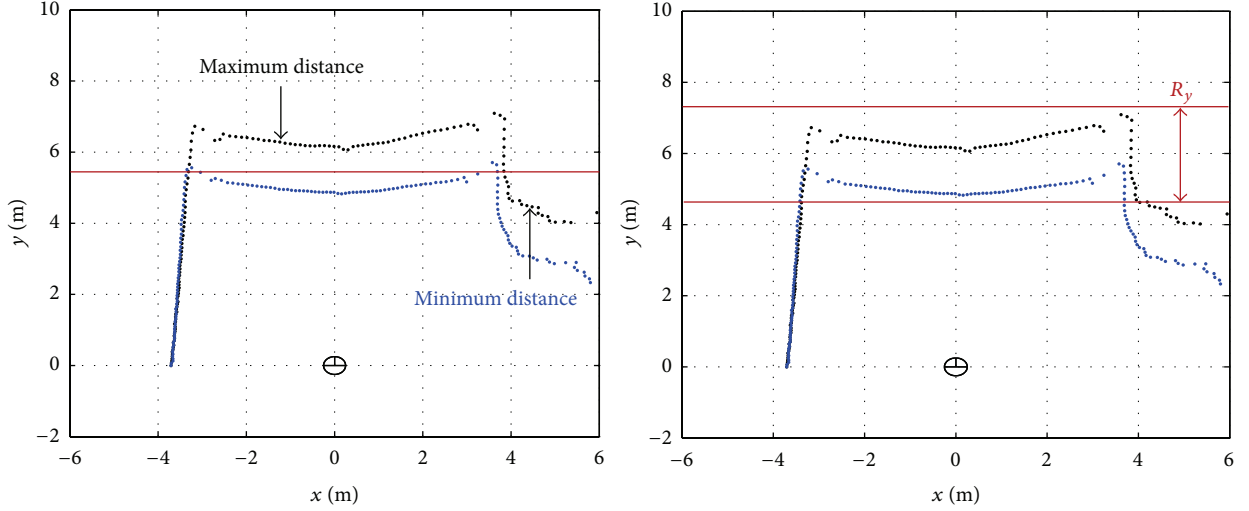
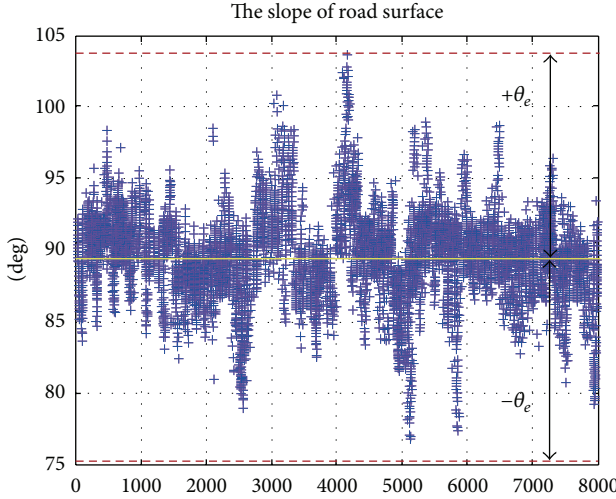
LRFs have been widely used. Rho et al. [15, 16] proposed an algorithm for detecting curbs by extracting the lines of a road surface using Hough transforms. Although the algorithm works well in many cases, the curbs and road surfaces have to be sufficiently flat because of the limitation of the Hough transform. In [17], an algorithm is presented for detecting the lines of curbs for some classes of environment using the Extended Kalman Filter (EKF). Kodagoda et al. [18–20] proposed a reliable curb detection algorithm based on the EKF. The algorithm was experimentally verified under a dynamic obstacle environment. LRF data have been obtained in 3D and used to detect the traversable area of the road [21]. However, traversable regions have been commonly detected using vision sensors. Nefian and Bradski [22] proposed a method of image segmentation based on the Bayesian network. An algorithm for detecting a traversable area using a homography segmentation has been presented [23]. Vision sensors, however, have difficulties in coping with bad weather

FIGURE 2: Definition of coordinates and variables. An LRF is mounted at tilt angle  $\Phi$ . Dotted line represents the nominal road surface. The shaded zone corresponds to the traversable region.FIGURE 3: Expected region of the road surface  $R_Y$ .

and illumination change. In [24], a traversable road extraction method was presented for autonomous robot navigation in outdoor cluttered pedestrian walkways. Multiple LRFs are required for implementation.

In this paper, we propose an algorithm for recognition of curbs, the road surfaces, and obstacles using a single LRF in various road conditions. At least one LRF is already installed for obstacle detection, so the proposed algorithm can be applied without additional costs. The traversable region is determined by the locations of curbs and obstacles in the robot's local coordinate. The robot can move safely if traversable region can be detected successfully, even when the localization accuracy is poor. The underlying idea of this study is to utilize the accurate range data of the LRF. Vision systems are excluded to guarantee reliable operation regardless of weather conditions. This paper presents a novel approach to the reliable recognition of road features. Several attributes are defined as geometric features. Experimental attribute data are collected, and the recognition algorithm is inductively established by using the Principal Component Analysis (PCA). The PCA in [25] provides the mathematical framework of combining multiple geometric attributes.

The rest of the paper is organized as follows. In Section 2, the traversable region detection algorithm is presented. Section 3 presents the experimental results of an outdoor

FIGURE 4: LRF data of the road surface and expected region of the road surface  $R_Y$ .FIGURE 5: Slope ( $\circ$ ) of the road surface and tolerance ( $\theta_e$ ) of the slope in robot coordinates.

mobile robot in the petroleum storage base environment. Some concluding remarks are presented in Section 4.

## 2. Traversable Region Detection Algorithm

**2.1. System Configuration.** Figure 2 presents the coordinate frames and the mounting configuration of the LRF. The fixed LRF looks down on the road at a small tilt angle  $\Phi$ . The scanning range is assumed to be  $180^\circ$ . Table 1 shows the nomenclature. Variables are described with respect to the robot coordinate. The traversable region corresponds to the road surface between the right and left curbs excluding obstacles.

The road surface points form a straight line if the ground is flat. However, more often, the range images of the road surface show generally curves because most of the road

surfaces are convex. The LRF measurements are affected by the vibration of the robot during motion. Curbs are typically two parallel lines in the range image. However, curb images become distorted for a curved road. There are many different shapes of curbs. In addition, there are no curbs at branches or intersections. Therefore, various uncertainties of LRF measurements should be considered.

The proposed algorithm is composed of three steps. The first step is to determine the pose of the robot with respect to the road surface points (road feature detection). The second step is to extract curbs (curb detection). The third step is to extract the traversable road region with consideration to obstacles (traversable road-region detection).

**2.2. Road Feature Detection.** The expected region of the road surface is presented in Figure 3. This is derived from the tolerance of the LRF pitch angle. Distribution of LRF data varies with the  $Y_L$ -axis as the robot moves along the road. In practice, these variations are caused by the unevenness of the road surface. In order to obtain the tolerance of the pitch angle, an experiment was conducted in the target environment shown in Figure 1. LRF data were accumulated while the robot was traveling. Figure 4 shows the selected LRF data which has minimum and maximum distances to the robot position. By using this information, we can assume the expected road region of the road surface,  $R_Y$ , as shown in right Figure 4. The tolerance  $\epsilon$  is derived from the expected road region of the road surface,  $R_Y$ , as indicated in Figure 3. Therefore, the tolerance  $\epsilon$  is determined as  $2^\circ$ .

In order to identify road surface points, the LRF data in the expected region are selected first. Then, consecutive points are clustered. If the robot moves forward on a straight and flat road, the cluster of the road surface points becomes a line. The slope of the road surface line is parallel with the  $X_R$ -axis in the ideal case. In practice, the slope of the point cluster may have some variations because of convex road surfaces or robot heading errors. The tolerance errors of heading angle can be determined by experiments in target environment.

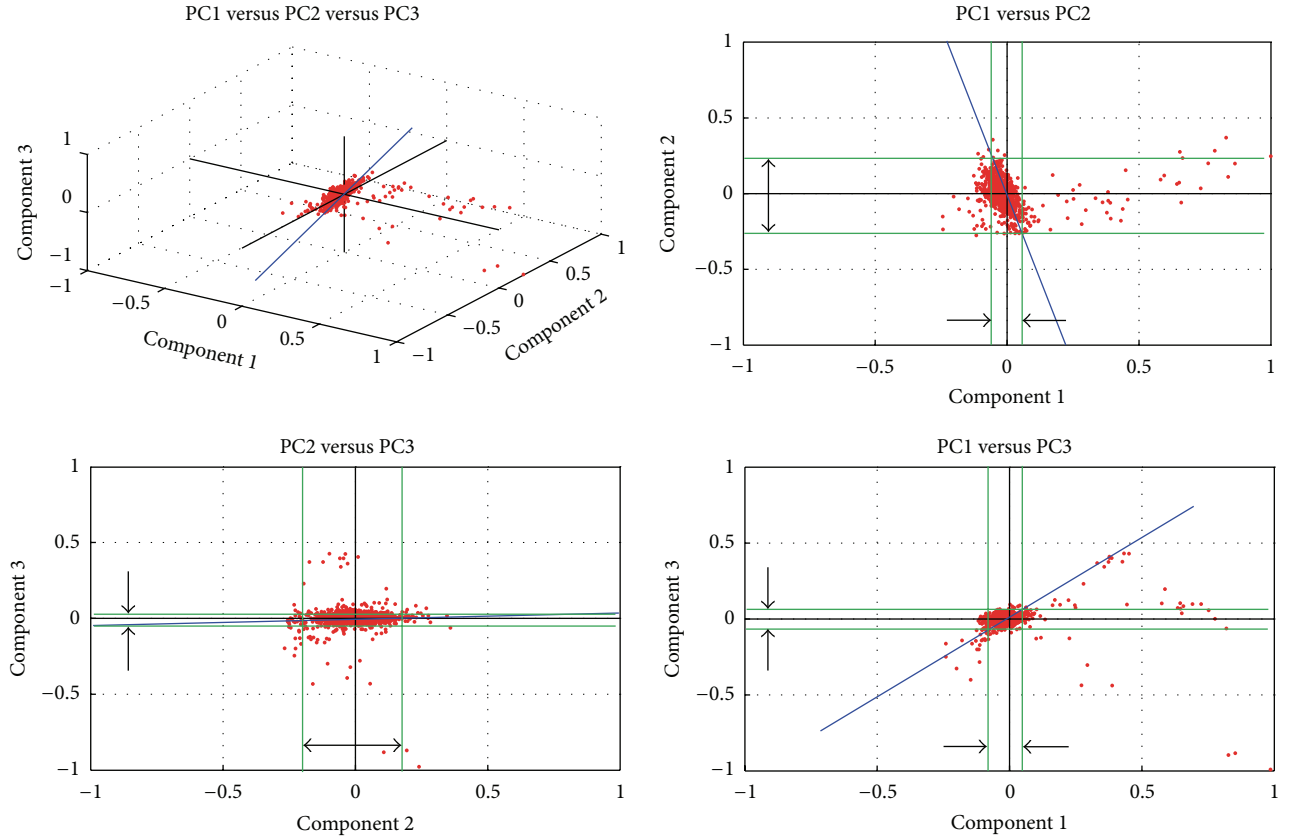


FIGURE 6: Selected principal axis in principal component space.

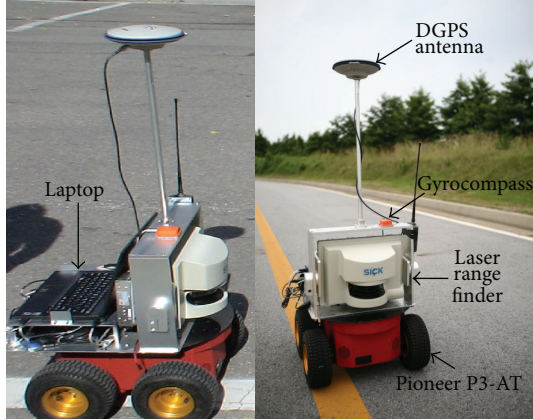


FIGURE 7: Robot platform.

Figure 5 shows the slope of the road surface with 8000 LRF data.

In Figure 5, the yellow line represents the average slope of the road surface, which is  $89.6^\circ$  close to  $90^\circ$ . Therefore, it can be concluded that the slope of the road surface is parallel to the  $X_R$ -axis. The red dotted line indicates the upper and lower bounds of the slope of the road surface. Therefore, the tolerance  $\pm\theta_e$  is determined as  $25^\circ$  by the difference between the upper and lower bounds. Finally, the extracted clusters

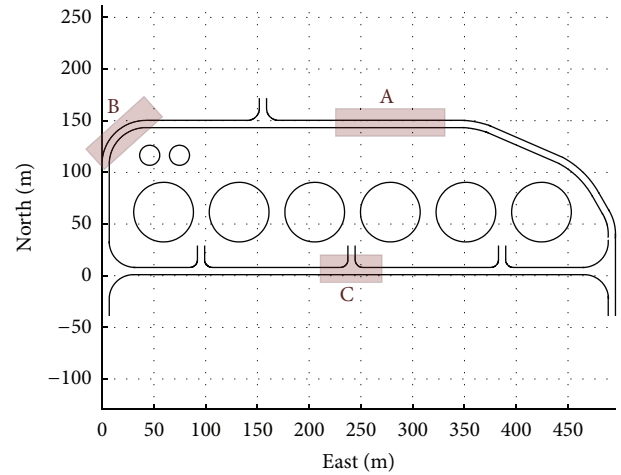


FIGURE 8: Target road environment of various road conditions, and a sector of the given area that is shown in Figure 1.

of the road surface points form the road surface. The road feature detection algorithm can be summarized as shown in Algorithm 1.

From the computed  $L_f$  in Algorithm 1, the road surface can be represented as one line using the conventional least square method. Angle  $\theta_f$  is the angle difference between the  $Y_R$ -axis and the derived line. The horizontal distance from the

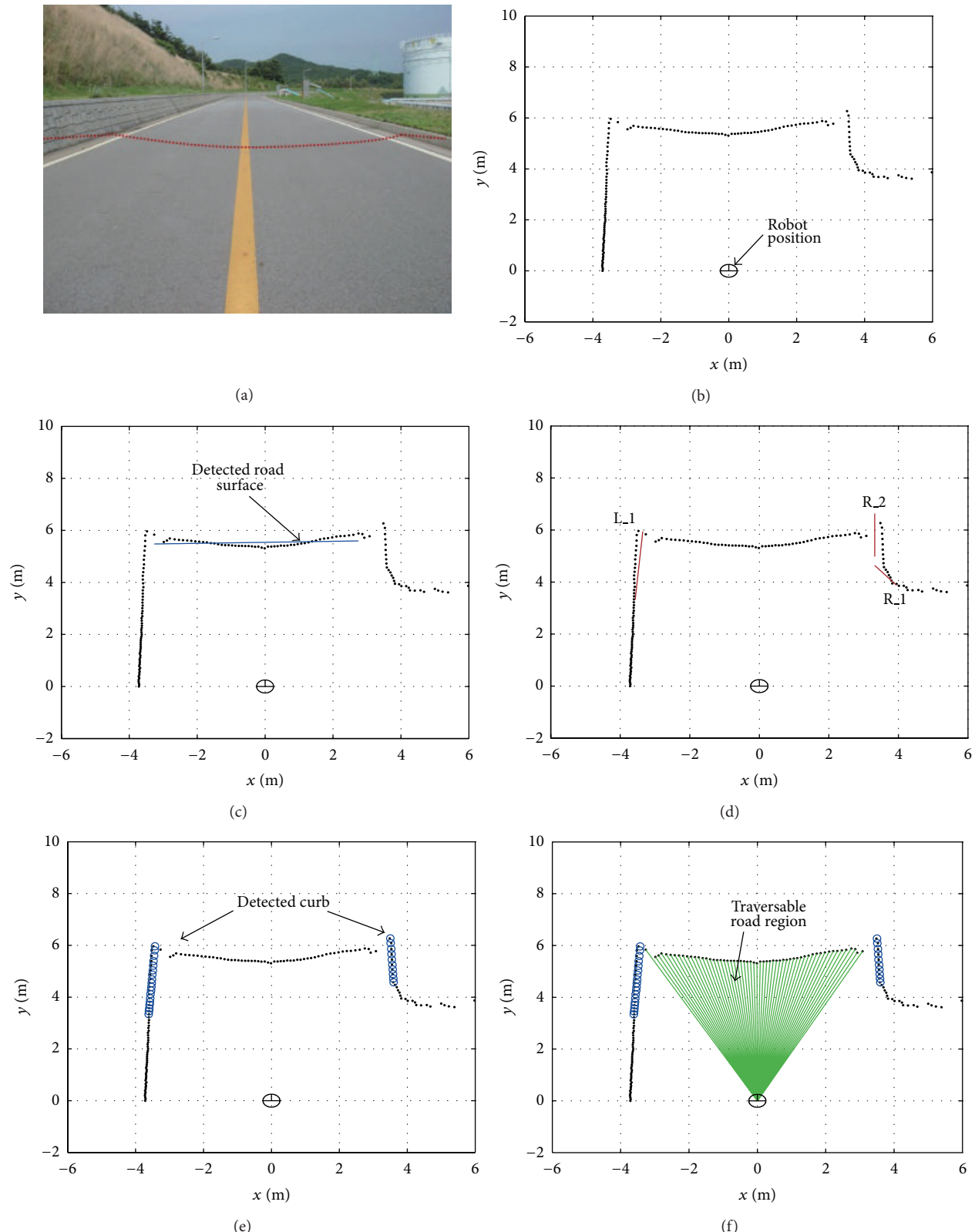


FIGURE 9: (a) Experimental environment; (b) LRF data; (c) detected road surface; (d) candidate curbs on the left and right; (e) detected curbs; (f) detected traversable road region.

```

(1)  $L_{X,k} \leftarrow$  x coordinate of the LRF measurement
(2)  $L_{Y,k} \leftarrow$  y coordinate of the LRF measurement
(3)  $N \leftarrow$  Count of the LRF measurement
(4) for  $k \leftarrow 1$  to  $N$ 
(5)   if  $L_{Y,k} \in R_Y$ 
(6)     then  $L_r \leftarrow$  Candidate for the road surface
(7)        $\theta_{L,r} \leftarrow$  Slope of candidate for the road surface
(8)        $M \leftarrow$  Count of candidate for the road surface
(9)   for  $l \leftarrow 1$  to  $M$ 
(10)  if  $\|\theta_{L,r}\| \leq \theta_e$ 
(11)    then  $L_f \leftarrow$  save  $L_r$  as the road surface
(12) return ( $L_f$ )

```

ALGORITHM 1: Computing the road feature properties.

```

(1) Select the first  $N$  points, construct a line by the use of a least square method in [14].
(2) Construct a line by employing the next  $N$  points.
(3) Compute Euclidean distance of two lines.
(4) If Euclidean distance is smaller than  $d_m$ , merge the lines and re-compute the line
parameters, continue (go to 2).
(5) Otherwise, return the line.
(6) Continue with the next  $N$  points, go to 2.

```

ALGORITHM 2: Line segmentation and clustering.

LRF origin to the road surface points is represented by  $d_f$ . The average value of  $y$  coordinates of the derived line.

**2.3. Curb Detection Using the Principal Component Analysis (PCA).** At first, by combining consecutive  $N$  LRF data, each line segment is constructed. Then, separate line segments are merged into one line when multiple line segments can be considered to be a single line. In order to evaluate the closeness of line segments, Euclidean distance is applied as introduced in [14]. Two line segments  $x_i = [\alpha_i \ r_i]^T$  and  $x_j = [\alpha_j \ r_j]^T$  in polar coordinate are merged when the Euclidean distance is smaller than threshold  $d_m$ . The validation process can be written as the following equation:

$$(x_i - x_j)^T (x_i - x_j) \leq d_m. \quad (1)$$

The procedure of line segmentation and clustering can be summarized as in Algorithm 2.

Extracted line clusters are considered as curb candidates.

We define several attributes from geometric features in order to extract curbs. The defined attributes are shown as follows.

- (Att\_1) The angular difference between the curb orientation  $\theta_c$  and road-surface slope  $\theta_f$ . This is close to  $90^\circ$ .
- (Att\_2) The gap between the road surface horizon distance  $d_f$  and the maximum  $y$  of the curb points. This is close to 0.
- (Att\_3) The angular difference between the left and the right curb orientations. This is close to 0.

(Att\_4) The range difference between the road width and the gap of two curbs. This is close to 0. It is assumed that the road width is known.

It is commonly assumed that the robot's heading is parallel with the curb orientation. However, this assumption becomes invalid when there is an inclination of the road surface. (Att\_1) extracts the candidate lines of both right and left curbs. The candidate lines are registered as curbs when the candidates satisfy the validation gate, which is a function of (Att\_2), (Att\_3), and (Att\_4). About (Att\_2), (Att\_3), and (Att\_4), we exploit the Principal Component Analysis (PCA) in order to define the validation gate. The PCA provides a mathematical procedure to combine three attributes as a linear combination. Therefore, the range of candidate curbs can be derived from these attributes with different dimensions. At last, prospective curbs can be selected from the candidate curbs within this range.

The validation gate is a scalar, and it is defined as a combination of attributes. There exists a unit vector  $u$  that can maximally represent all components. The vector  $u$  is defined as the principal axis that reduces the dimensions of the attribute space. In order to reduce the dimensions of attributes to  $k$  (where  $k < n$ ), each attribute should be normalized first:

$$\mu = \frac{1}{m} \sum_{i=1}^m x^{(i)} \quad x^{(i)} - \mu \quad (2)$$

$$\sigma_j^2 = \frac{1}{m} \sum_{i=1}^m (x_j^{(i)})^2, \quad x_j^{(i)} = \frac{x_j^{(i)} - \mu}{\sigma_j} \quad (3)$$

```

(1)  $L_{X,k} \leftarrow x$  coordinate of the LRF measurement
(2)  $L_{Y,k} \leftarrow y$  coordinate of the LRF measurement
(3)  $d_f \leftarrow$  Horizontal distance to road surface
(4)  $N \leftarrow$  Count of the LRF measurement
(5) for  $k \leftarrow 1$  to  $N$ 
(6)   if  $L_{X,k} \leq d_{C,R}$  and  $L_{X,k} \geq -d_{C,L}$ 
(7)     if  $L_{Y,k} \leq d_f$ 
(8)       then  $L_{\text{obstacle}} \leftarrow$  Obstacle data set
(9)     else  $L_{\text{pass}} \leftarrow$  Add  $L_{X,k}$  and  $L_{Y,k}$  to the traversable
           region, data set  $(X_{\text{pass}}, Y_{\text{pass}})$ 
(10) return  $(L_{\text{pass}})$ 

```

ALGORITHM 3: Detect the traversable road region.

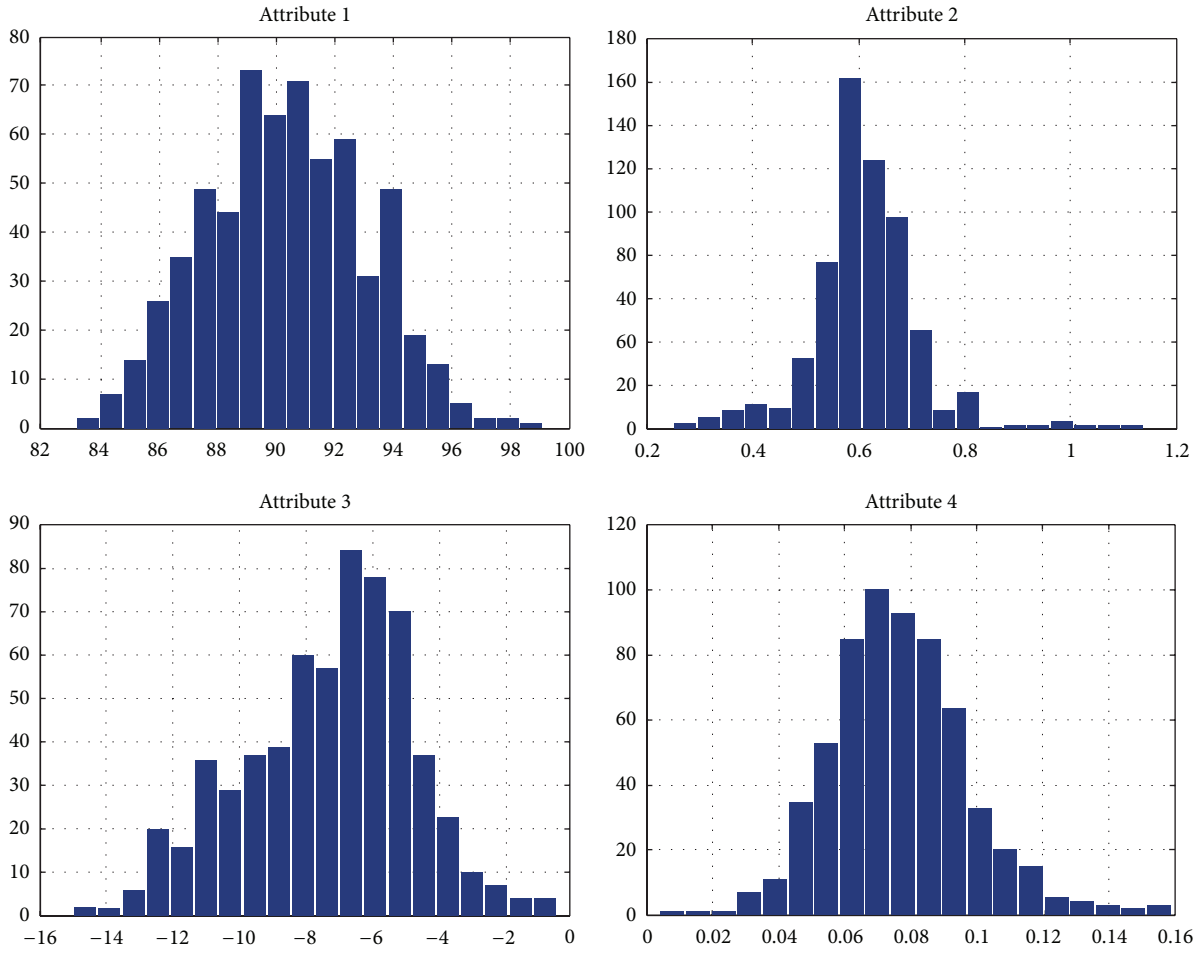


FIGURE 10: PCA attributes in straight road environment.

Means are shifted to 0 by (2). Equation (3) is the rescaling process. The unit vector  $u$  can be derived from the following equation:

$$\begin{aligned} \frac{1}{m} \sum_{j=1}^m (x^{(i)T} u)^2 &= \frac{1}{m} \sum_{i=1}^m u^T x^{(i)} x^{(i)T} u \\ &= u^T \left( \frac{1}{m} \sum_{j=1}^m x^{(i)} x^{(i)T} \right) u. \end{aligned} \quad (4)$$

The unit vector  $u$  is defined from the eigenvector and the eigenvalue of the covariance matrix  $\Sigma = (1/m) \sum_{j=1}^m x^{(i)} x^{(i)T}$  by the following equation:

$$\begin{aligned} u^T \Sigma u &= u^T \lambda u = \lambda u^T u = \lambda \\ \Sigma u &= \lambda u. \end{aligned} \quad (5)$$

In (5),  $u$  is the eigenvector of the covariance matrix  $\Sigma$ , and  $\lambda$  is the eigenvalue. The principal axis corresponds to

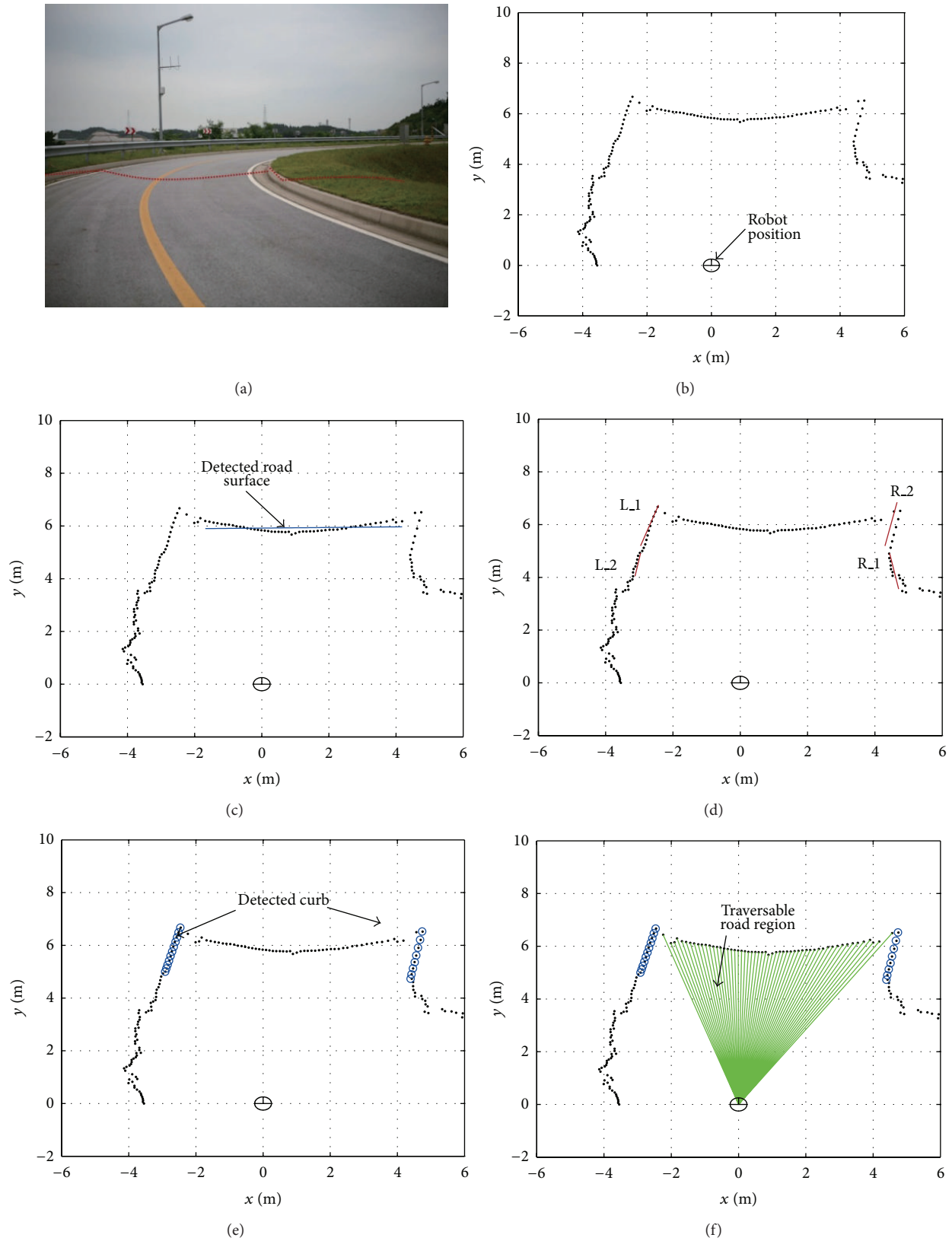


FIGURE 11: (a) Experimental environment; (b) LRF data; (c) detected road surface; (d) candidate curbs on the left and right; (e) detected curbs; (f) detected traversable road region.

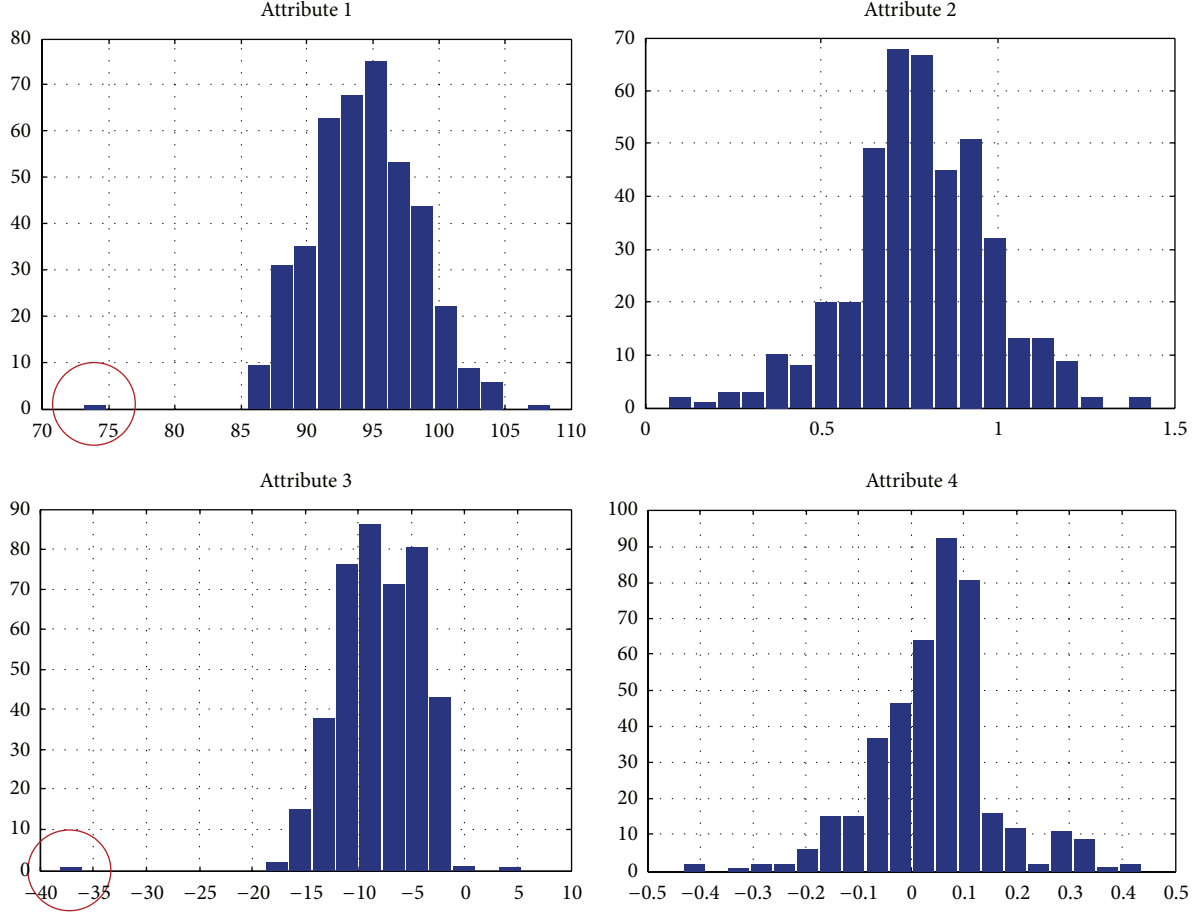


FIGURE 12: PCA attributes in straight road environment.

the eigenvector with the largest eigenvalue. Figure 6 shows the computational result of the PCA algorithm. The blue line represents the selected principal axis, and the green dotted line is the range of the principal axis which can be selected as curbs. The red dots represent the principal component.

The experimental measurements are obtained from a test run in the environment in Figure 1. From LRF measurements, 999 candidate lines were extracted. The principal axis  $u$  is shown in the principal component space. The validation gate  $Vg$  can be defined by the following equation:

$$Vg = u_1 \cdot X_1 + u_2 \cdot X_2 + u_3 \cdot X_3. \quad (6)$$

A reliable curb recognition algorithm can be obtained by appropriate selection of the range of  $Vg$  results.  $X_1$ ,  $X_2$ , and  $X_3$  correspond to the principal components of attributes (Att\_2), (Att\_3), and (Att\_4), respectively. The range of the principal component is determined by comparing the collected data of the curbs with the expected values. The derived range is used for obtaining the acceptable ranges of attributes from the experimental results and represented as the green line in Figure 6. Table 2 summarizes the acceptable ranges of attributes from the experimental results.

**2.4. Traversable Region and Obstacle Detection.** LRF data within the range between the left curb ( $d_{C,L}$ ) and the right

TABLE 2: Acceptable range of curb attributes.

	Att.2 [m]	Att.3 [deg]	Att.4 [m]
Max.	1.5	20	0.5
Min.	0.1	-20	-0.5

TABLE 3: Selection of curbs (values resulting from (6)).

	R_1	R_2
L_1	4.29	0.86

TABLE 4: Selection of curbs (values resulting from (6)).

	R_1	R_2
L_1	1.79	1.75
L_2	1.92	1.88

TABLE 5: Selection of curbs (values resulting from (6)).

	L_1	L_2
R_1	1.19	1.37

curb ( $d_{C,R}$ ) are determined as the expected region. This region is used to detect obstacles and traversable area. If the

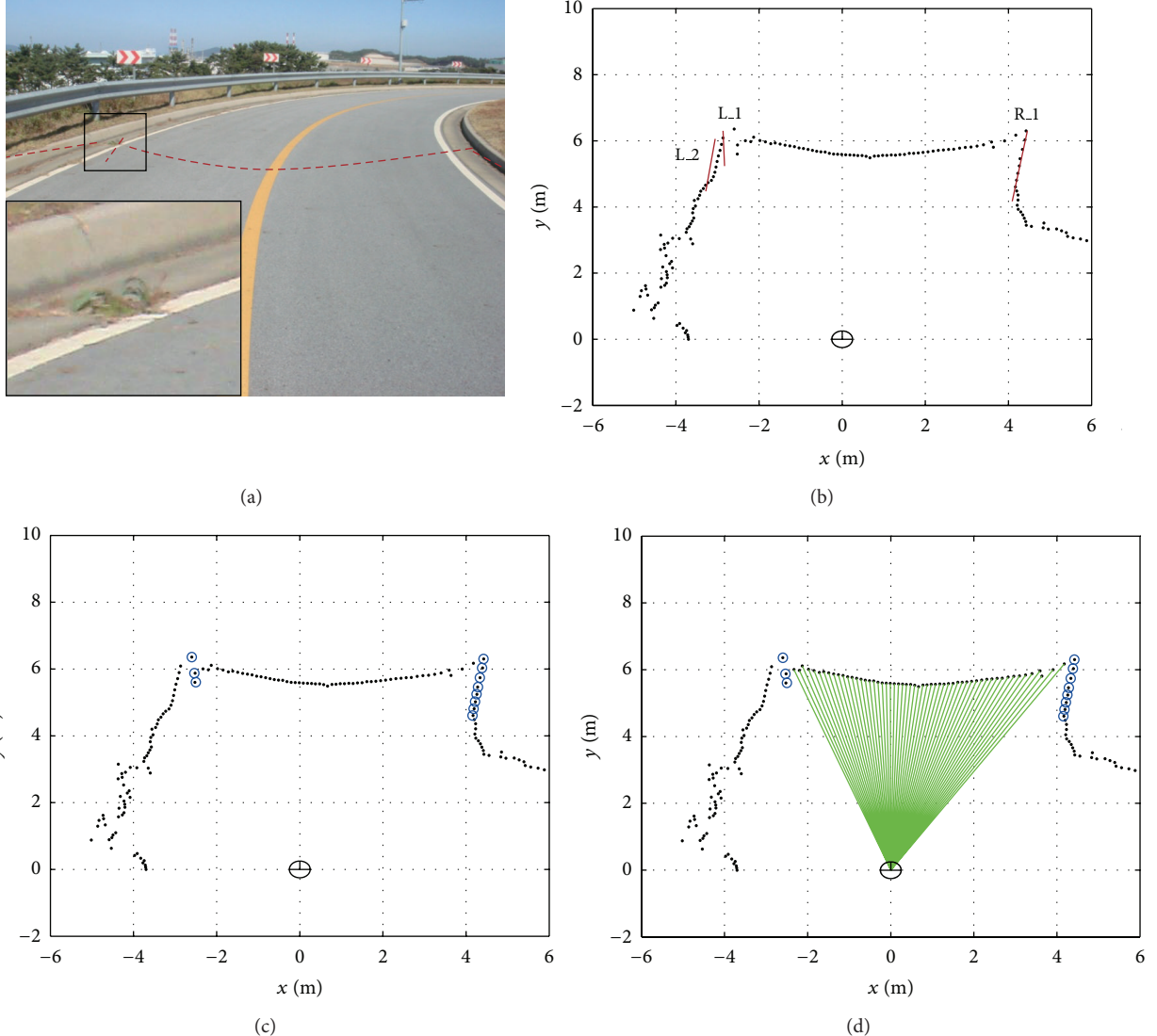


FIGURE 13: (a) Road environment with weeds; (b) candidate curbs on the left and right; (c) detected weeds as the curb; (d) detected traversable road region.

TABLE 6: Expected obstacle region.

	Min. value, m	Max. value, m
X range	-3.58	3.56
Y range	0	3.73

TABLE 7: Expected obstacle region.

	Min. value, m	Max. value, m
X range	-3.41	3.71
Y range	0	3.92

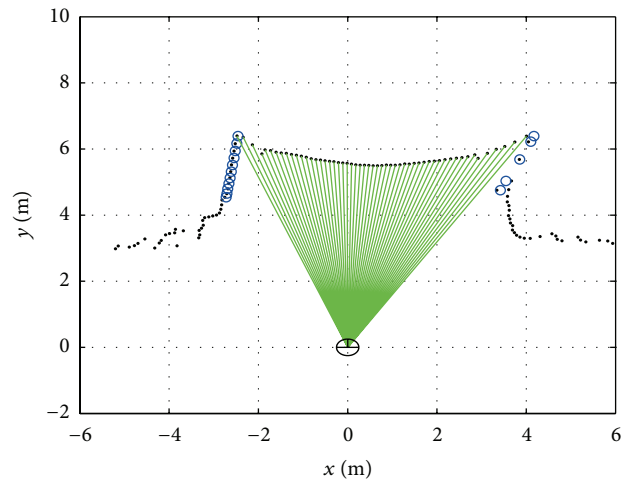
$y$  value of LRF data is lower than  $d_f$ , the data represents an obstacle. The expected region without obstacles is considered as a traversable area. The algorithm also enables the robot to calculate the traversable area regardless of curbs by assuming

the locations of the curbs when the value of the road's width is given. The algorithm for the condition in which both left and right curbs exist is as in Algorithm 3.

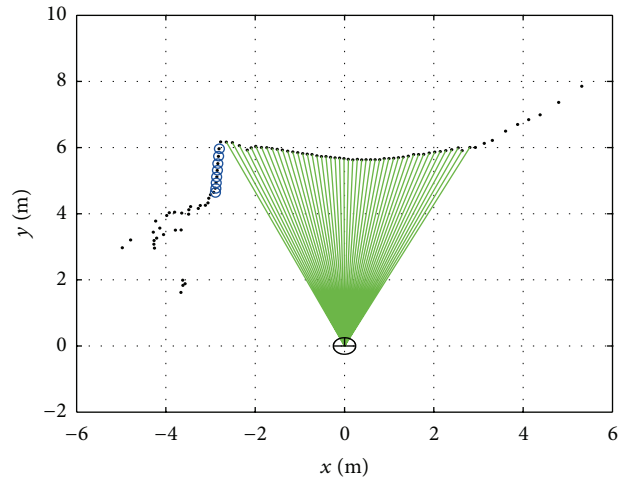
Detected traversable region can guarantee the safety of outdoor navigation regardless of the localization performance since it guides the robot in a safe drive direction in the robot coordinate system. Therefore, this method can also be used for local obstacle avoidance such as VFH [26].

### 3. Experimental Results

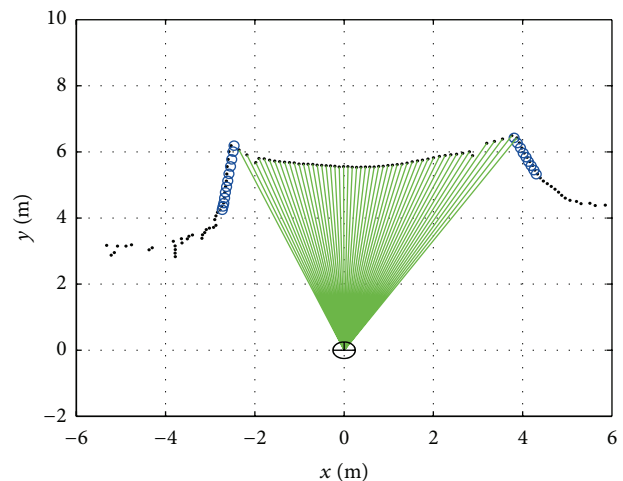
**3.1. Experimental Setup.** Figure 7 shows the experimental setup. We constructed the navigation system on a P3-AT model of pioneer. It is a four-wheeled robot designed for outdoor use with odometry. A SICK laser sensor (LMS200 in [27]) is mounted on the robot to detect the range around the robot. The maximum range of the LRF is 33 m, and its static



(a)



(b)



(c)

FIGURE 14: Experimental environment and detected curbs and traversable region on a fork in the road in robot coordinates.

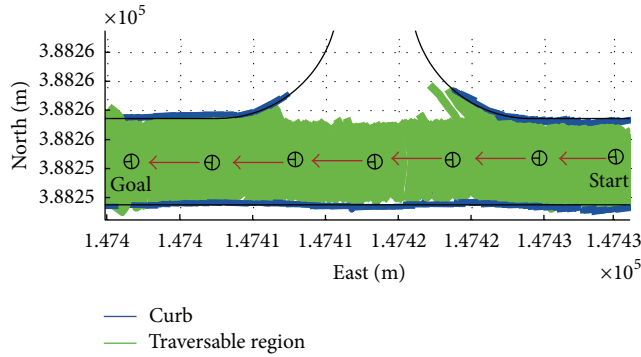


FIGURE 15: Detected curbs and traversable region on a fork in the road in global coordinates.

error is under 0.3 cm. To detect the road surfaces and curbs, the LRF was mounted at a small tilt angle  $6.4^\circ$ . The Novatel DGPS system was attached to localize the robot and the Xsens gyrocompass sensor was used to obtain the direction of the robot. Computations were conducted by a laptop.

The proposed algorithm is applied to the various road environments in petroleum storage bases. Figure 8 presents the setting of the targeted roads in global coordinates. In order to test the robot's performance in various conditions, three different types of roads were selected from the experiment site: a straight road, area A; a curved road, area B; and a forked road, area C. The widths of the roads are between 6 m and 7 m, and the robot traveled in a clockwise direction.

Experiment I was conducted in area A, a straight road with the width of 7 m. While the robot traveled in area A, curbs and traversable area were detected by LRF applying the proposed algorithm. Experiment II was carried out in area B, a curved road with the width of 6 m. Experiment III was conducted on a fork in the road of 6 m in width, area C. In Experiment III, as the robot traveled in a clockwise direction, the curbs on the right side disappeared and thus became undetectable. Experiment IV was carried out in area A with obstacles. The results of robot navigation in these environments are presented as follows.

**3.2. Experiment I.** As shown in Figure 8 in experiment I, the robot traveled approximately 100 m following the straight center line in area A of the straight road environment. Curbs existed on both sides of the road. While driving, 600 LRF data were acquired. Figure 9 shows the process of the algorithm with the LRF data. In Figure 9(a), the environment setting is presented, and the red dotted line represents the positions of the obtained LRF data. These LRF data are shown in robot coordinate in Figure 9(b). Figure 9(c) shows the result of detected road surface represented as a blue line. Figure 9(d) shows the candidate curbs on both sides of the road. Left and right sides are determined by the heading of the robot,  $Y_R$  axis. There is one candidate curb (L<sub>1</sub>) on the left and two candidate curbs (R<sub>1</sub>, R<sub>2</sub>) on the right. With the attributes of each candidate, the value of Vg is derived from the PCA method. The candidate curbs with the lowest value of Vg are selected as curbs. Therefore, L<sub>1</sub> and R<sub>2</sub> are detected as

curbs as shown in Figure 9(e). The calculated values of Vg are indicated in Table 3. Figure 9(f) shows the result of detected traversable road region.

The histograms illustrating the PCA attributes of detected curbs from the results of experiment I are shown in Figure 10. The average value of (Att<sub>1</sub>) is  $90.07^\circ$ . This result meets the environmental condition that the angular difference between curb orientation and road-surface slope is almost perpendicular. Other attributes are also in acceptable ranges of curb attributes as shown in Table 2. Distribution of (Att<sub>2</sub>) is between 0.2 m and 1.2 m, which is within the acceptable range of (Att<sub>2</sub>), between 0 m and 1.5 m. The average value of (Att<sub>3</sub>) is  $-7.5^\circ$ , and the distribution is between  $-7.5^\circ$  and  $0^\circ$  within the acceptable range of (Att<sub>3</sub>). The average value of (Att<sub>4</sub>) is 0.07 m, and the distribution is between 0 m and 0.16 m within the acceptable range of (Att<sub>4</sub>). These results prove that experiment I was conducted successfully for detecting curbs in area A. Also, the processing time of the algorithm between steps was 76 ms on average.

**3.3. Experiment II.** In experiment II, the robot traveled in area B of the curved road environment. Curbs exist on both sides of the road. While traveling, 418 LRF data were accumulated. Figure 11 presents the process of the algorithm with the LRF data in experiment II. In Figure 11(a), the experimental environment is presented, and red dotted line represents the positions of obtained LRF data. These LRF data are plotted in robot coordinate as shown in Figure 11(b). Figure 11(c) shows the result of detected road surface as a blue line. In Figure 11(d), candidate curbs can be seen on both sides of the road. There are two candidate curbs (L<sub>1</sub>, L<sub>2</sub>) on the left and two candidate curbs (R<sub>1</sub>, R<sub>2</sub>) on the right. With the attributes of each candidate, the value of Vg was derived from PCA method. As shown in Figure 11(e), among all candidate curbs, the curbs with the lowest value of Vg, L<sub>1</sub> and R<sub>2</sub>, are selected. The calculated values of Vg are indicated in Table 4. Figure 11(f) shows the result of detected traversable road region.

Figure 12 shows the histograms illustrating the PCA attributes of detected curbs from the results of experiment II. All the attributes except for (Att<sub>1</sub>) are within the acceptable ranges of curb attributes as shown in Table 2. Because experiment II was conducted on a curve, the difference in angle between curb orientation and road-surface slope is not clearly perpendicular. Thus, the average value of (Att<sub>1</sub>) is  $93^\circ$ . Distribution of (Att<sub>2</sub>) is between 0 m and 1.5 m, which are within the acceptable range of (Att<sub>2</sub>). The average value of (Att<sub>3</sub>) is  $-12^\circ$ . This result shows that the difference in angle between the left and the right curb orientations is larger on curved roads than on straight road. The average value of (Att<sub>4</sub>) is 0.07 m, and the distribution is between 0 m and 0.16 m in the acceptable range of (Att<sub>4</sub>). These results show that experiment II was conducted successfully for detecting curbs in area B.

Figure 13 presents the failure case of curb detection that the robot misclassifies the weeds on the road as curbs. This result can be seen as a red circle in Figure 12. The weeds can be found near the left curb as shown in Figure 13(a). Figure 13(b)

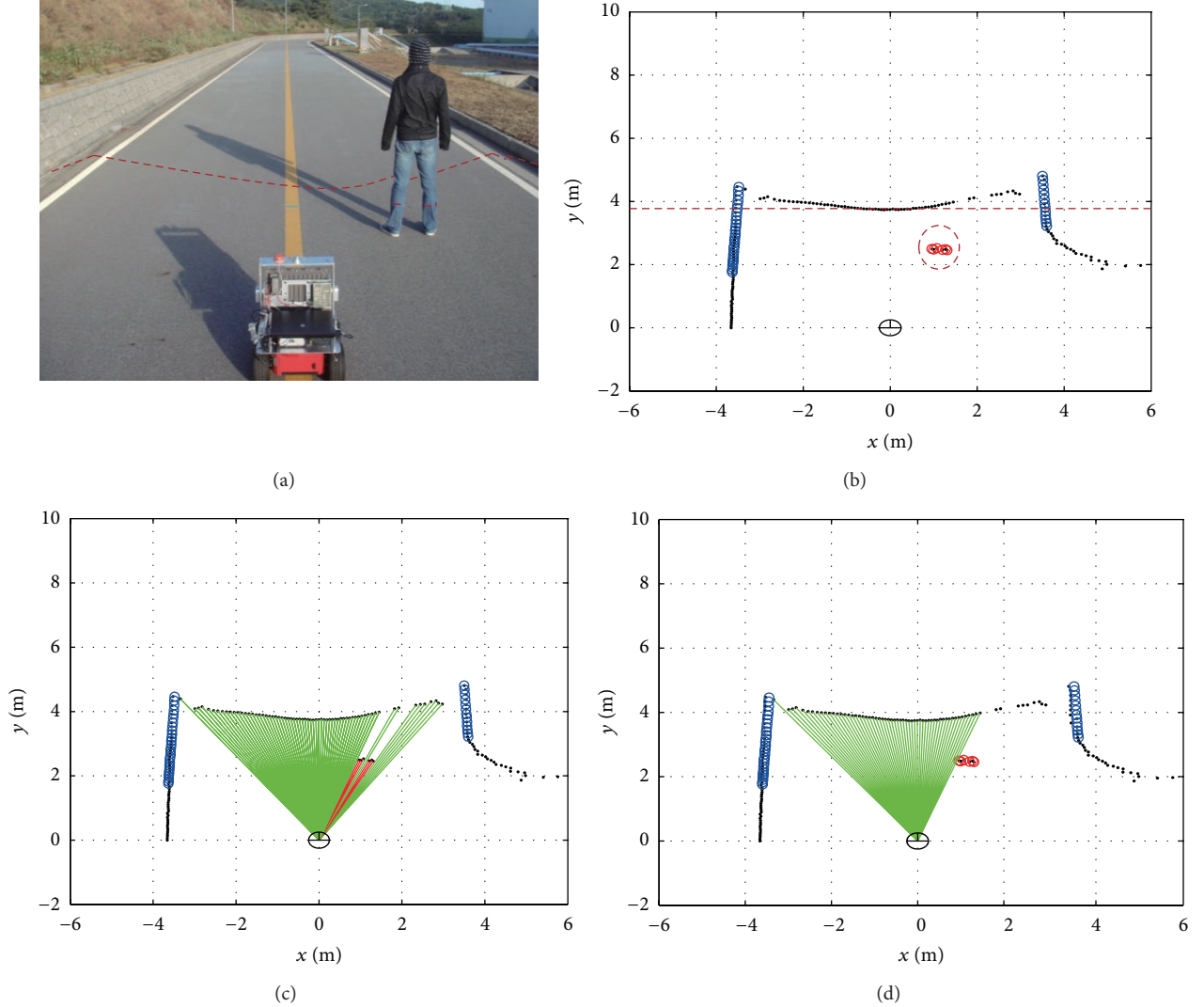


FIGURE 16: (a) Experimental environment; (b) detected curbs and obstacle; (c) candidates of traversable region; (d) detected traversable region.

shows the candidate curbs in this environment. There are two candidate curbs (L<sub>1</sub>, L<sub>2</sub>) on the left, and there is a candidate curb (R<sub>1</sub>) on the right. The calculated values of V<sub>g</sub> in (6) are shown in Table 5. Pair (L<sub>1</sub>, R<sub>1</sub>) is selected as curbs because of the lowest V<sub>g</sub>. This is a misclassification because the true curb pair is (L<sub>2</sub>, R<sub>1</sub>). The number of misclassifications was only one during the movement in area B shown in Figure 8. This result implies the 99.8% success rate (417 success/418 LRF scans). Therefore, partial failure was not a significant concern in practical applications.

**3.4. Experiment III.** Experiment III was conducted in area C of a fork in the road with the width of 6 m. In this road environment, the robot could not detect curbs on the right side while traveling in a clockwise direction. The robot traveled about 50 m and obtained 351 LRF data. Figure 14(a) presents the LRF data obtained as the robot approached the fork. As shown in Figure 14(b), even when curbs disappeared on the right side of the road while traveling, the robot was able

to detect the traversable region successfully since the width of the road was 6 m, and the information of curbs on the left side was given. Figure 14(c) shows LRF data collected by the robot as it passed by the fork.

Figure 15 shows these results, which were transformed into global coordinates. The blue line in Figure 15 indicates the detected curbs, and the green area presents the detected traversable region. Localization of the robot was estimated by the EKF algorithm using odometry data, DGPS, and gyroscope. In Figure 15, the location of the robot is plotted every 40 steps, and the detected curbs are plotted every 5 steps. These results show that experiment III was conducted successfully for detecting the traversable region and the curbs on the left side. The processing time of the algorithm between steps was 90 ms on average.

**3.5. Experiment IV.** In order to verify the algorithm in the obstacle environment, Experiment IV was carried out in area A. Figure 16 shows the experimental results of detected

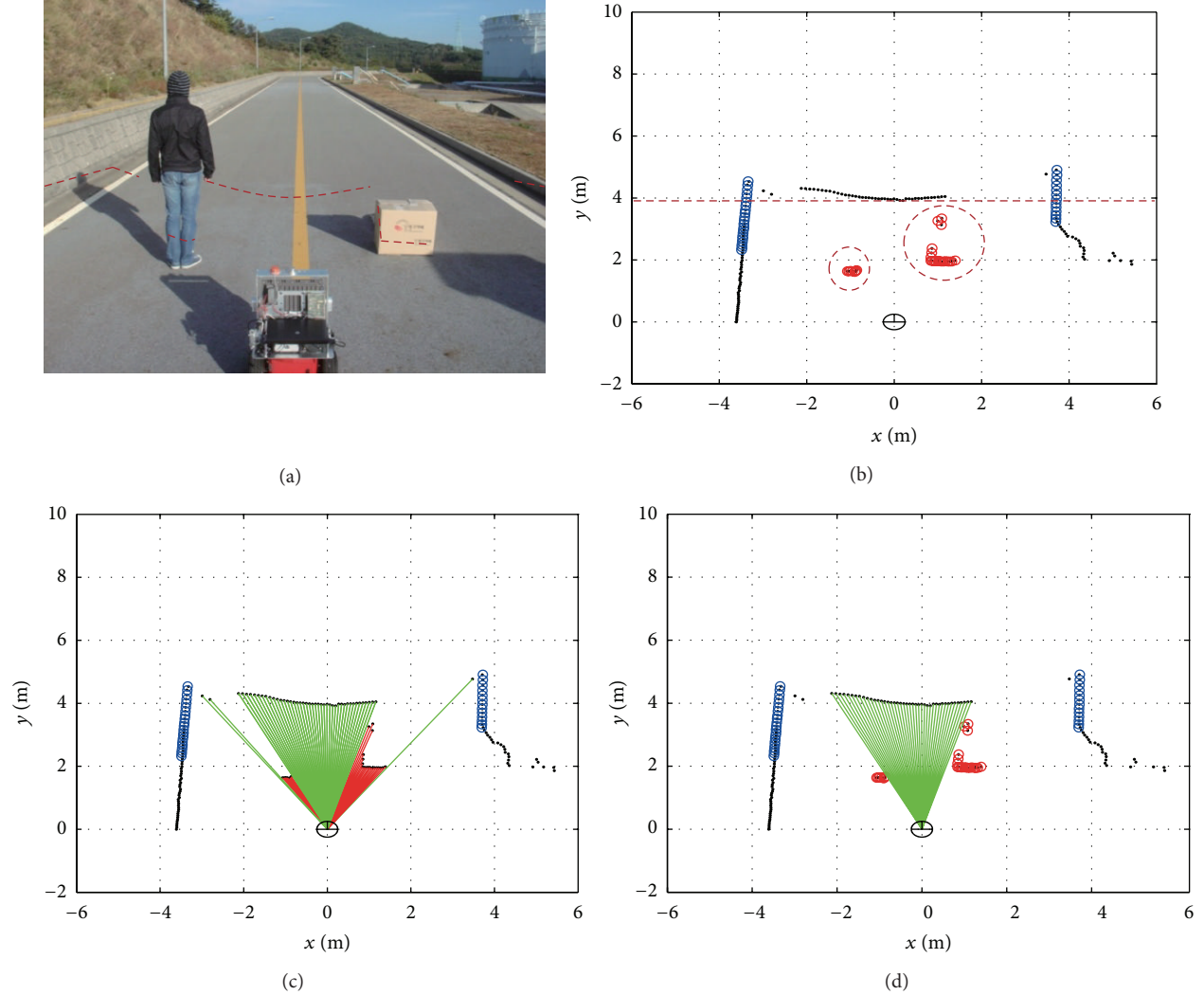


FIGURE 17: (a) Experimental environment; (b) detected curbs and obstacles; (c) candidates of traversable region; (d) detected traversable region.

traversable region when one pedestrian exists. The red dotted line represents the scanning area of LRF. The curbs are represented in blue lines as shown in Figure 16(b). The horizontal distance  $d_f$  in Table 1 is shown in the red dashed line. The expected obstacle region is determined by the detected curbs and  $d_f$  as indicated in Table 6. The LRF data lying on this region are considered as an obstacle. The red circled data in Figure 16(b) indicate the detected obstacle that corresponds to the pedestrian. From the road surface and the obstacle, the candidates of traversable region are obtained as shown in Figure 16(c). The green regions indicate the candidates of the traversable region, and the red regions show the collision region due to the detected obstacle. Among these candidates of the traversable region, the region with the widest width is finally selected for safety. The finally detected traversable region is shown in Figure 16(d).

Figure 17 shows the experimental results, when one pedestrian and a box exist. The experimental environment is shown in Figure 17(a). The expected obstacle region is

determined by the curbs and the road surface as indicated in Table 7. The LRF data marked by the red circle in Figure 17(b) are considered as obstacles that correspond to a pedestrian and a box, respectively. The candidates of the traversable region are shaded as the green regions. The collision regions due to the obstacles are represented by the red regions. The candidate region that has the widest width is selected as the traversable region.

#### 4. Conclusion

In this paper, we proposed a method that can address the perceptual issues related to outdoor road environments for outdoor navigation. We used a single laser range finder to detect curbs, road surfaces, and obstacles. Hence, this method can be easily adopted for practical applications. By extracting two types of information (on curbs and road surfaces), we increased the reliability of traversable road

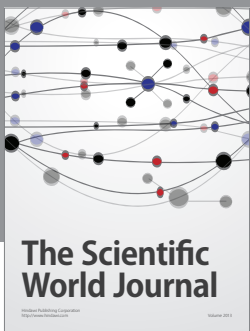
detection in relation to the findings of other studies. This method, in combination with the pose estimation method, was verified by experiments for various road environments. This algorithm was computationally efficient and guaranteed the safety of outdoor navigation. Since there are many potential applications of autonomous outdoor mobile robots in semistructured road environments, the proposed method can be widely used as a low-cost practical solution for safe outdoor navigation.

## Acknowledgments

This work was supported by the NRF Grant funded by the MEST, Korea (2013-029812). This research was also supported in part by the MKE, Korea, under the Human Resources Development Program supervised by the NIPA (NIPA-2013-H1502-13-1001). The research was also supported in part by the Implementation of Technologies for Identification, Behavior, and Location of Human based on Sensor Network Fusion Program through the MKE (Grant no. 10041629).

## References

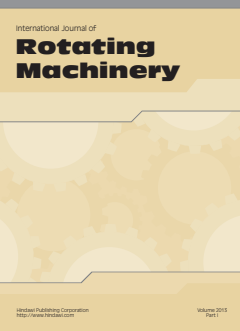
- [1] B. Kim, J. Park, S. Park, and S. Kang, "Impedance learning for robotic contact tasks using natural actor-critic algorithm," *IEEE Transactions on Systems, Man, and Cybernetics, Part B*, vol. 40, no. 2, pp. 433–443, 2010.
- [2] S. Kang, K. Komoriya, K. Yokoi, T. Koutoku, B. Kim, and S. Park, "Control of impulsive contact force between mobile manipulator and environment using effective mass and damping controls," *International Journal of Precision Engineering and Manufacturing*, vol. 11, no. 5, pp. 697–704, 2010.
- [3] B. Chu, D. Kim, and D. Hong, "Robotic automation technologies in construction: a review," *International Journal of Precision Engineering and Manufacturing*, vol. 9, no. 3, pp. 85–91, 2008.
- [4] B. Chu, K. Jung, C.-S. Han, and D. Hong, "A survey of climbing robots: locomotion and adhesion," *International Journal of Precision Engineering and Manufacturing*, vol. 11, no. 4, pp. 633–647, 2010.
- [5] Y.-J. Lee and J.-B. Song, "Three-dimensional iterative closest point-based outdoor SLAM using terrain classification," *Intelligent Service Robotics*, vol. 4, no. 2, pp. 147–158, 2011.
- [6] X. Zhang, M. Geimer, P. O. Noack, and L. Grandl, "A semi-autonomous tractor in an intelligent master-slave vehicle system," *Intelligent Service Robotics*, vol. 3, no. 4, pp. 263–269, 2010.
- [7] M. Buehler, K. lagnemma, and S. Singh, Eds., *The 2005 DARPA Grand Challenge*, Springer, 2007.
- [8] M. Buehler, K. lagnemma, and S. Singh, Eds., *The DARPA Urban Challenge: Autonomous Vehicles in City Traffic*, Springer, 2010.
- [9] H. Dahlkamp, A. Kaehler, D. Stavens, S. Thrun, and G. Bradski, *Self-Supervised Monocular Road Detection in Desert Terrain*, Robotics Science and Systems, Philadelphia, Pa, USA, 2006.
- [10] S. J. Velat, J. Lee, N. Johnson, and C. D. Crane III, "Vision based vehicle localization for autonomous navigation," in *Proceedings of the IEEE International Symposium on Computational Intelligence in Robotics and Automation (CIRA '07)*, pp. 528–533, June 2007.
- [11] R. Wang, Y. Xu, Libin, and Y. Zhao, "A vision-based road edge detection algorithm," in *Proceedings of the IEEE Intelligent Vehicle Symposium*, vol. 1, pp. 141–147, June 2002.
- [12] Q. B. Truong, B. R. Lee, N. G. Heo, Y. J. Yum, and J. G. Kim, "Lane boundaries detection algorithm using vector lane concept," in *Proceedings of the 10th International Conference on Control, Automation, Robotics and Vision (ICARCV '08)*, pp. 2319–2325, Hanoi, Vietnam, December 2008.
- [13] B.-F. Wu and C.-T. Lin, "Robust lane detection and tracking for driving assistance systems," in *Proceedings of the IEEE International Conference on Systems, Man, and Cybernetics (SMC '07)*, pp. 3848–3853, Montréal, Canada, October 2007.
- [14] R. Siegwart and I. R. Nourbakhsh, *Autonomous Mobile Robots*, MIT Press, Cambridge, Mass, USA, 2004.
- [15] C.-W. Roh, S.-H. Kim, M.-J. Kim, S.-C. Kang, and S.-K. Hong, "Development of patrol robot using DGPS and curb detection," *International Journal of Control, Automation and Systems*, vol. 13, pp. 140–146, 2007.
- [16] S.-H. Kim, C.-W. Roh, S.-C. Kang, and M. Park, "Curb detection using laser range finder for reliable outdoor navigation," in *Proceedings of the IEEE International Conference on Advanced Robotics (ICAR '07)*, pp. 930–935, Jeju, Republic of Korea, 2007.
- [17] C. Yu and D. Zhang, "Road curbs detection based on laser radar," in *Proceedings of the 8th International Conference on Signal Processing (ICSP '06)*, Guilin, China, November 2006.
- [18] W. S. Wijesoma, K. R. S. Kodagoda, and A. P. Balasuriya, "Road-boundary detection and tracking using lidar sensing," *IEEE Transactions on Robotics and Automation*, vol. 20, no. 3, pp. 456–464, 2004.
- [19] K. R. S. Kodagoda, W. S. Wijesoma, and A. P. Balasuriya, "Road curb and intersection detection using a 2D LMS," in *Proceedings of the IEEE/RSJ International Conference on Intelligent Robots and Systems (IROS '02)*, pp. 19–24, Lausanne, Switzerland, October 2002.
- [20] W. S. Wijesoma, K. R. S. Kodagoda, A. P. Balasuriya, and E. K. Teoh, "Road edge and lane boundary detection using laser and vision," in *Proceedings of the IEEE/RSJ International Conference on Intelligent Robots and Systems (IROS '01)*, pp. 1440–1445, Maui, Hawaii, USA, November 2001.
- [21] Y. Morales, A. Carballo, E. Takeuchi, A. Aburadani, and T. Tsubouchi, "Autonomous robot navigation in outdoor cluttered pedestrian walkways," *Journal of Field Robotics*, vol. 26, no. 8, pp. 609–635, 2009.
- [22] A. V. Nefian and G. R. Bradski, "Detection of drivable corridors for off-road autonomous navigation," in *Proceedings of the IEEE International Conference on Image Processing (ICIP '06)*, pp. 3025–3028, October 2006.
- [23] C. Guo and S. Mita, "Drivable road region detection based on homography estimation with road appearance and driving state models," in *Proceedings of the 4th International Conference on Autonomous Robots and Agents (ICARA '09)*, pp. 204–209, February 2009.
- [24] B. Ma, S. Lakshmanan, and A. O. Hero III, "Simultaneous detection of lane and pavement boundaries using model-based multisensor fusion," *IEEE Transactions on Intelligent Transportation Systems*, vol. 1, no. 3, pp. 135–147, 2000.
- [25] I. T. Jolliffe, *Principal Component Analysis*, Springer, New York, NY, USA, 2nd edition, 2002.
- [26] J. Borenstein and Y. Koren, "The vector field histogram—fast obstacle avoidance for mobile robots," *IEEE Transactions on Robotics and Automation*, vol. 7, no. 3, pp. 278–288, 1991.
- [27] S. Thrun, W. Burgard, and D. Fox, *Probabilistic Robotics*, MIT Press, Cambridge, Mass, USA, 2005.



**The Scientific  
World Journal**



**Journal of  
Electrical and Computer  
Engineering**



**International Journal of  
Rotating  
Machinery**



**Active and Passive  
Electronic Components**



**Advances in  
Mechanical  
Engineering**

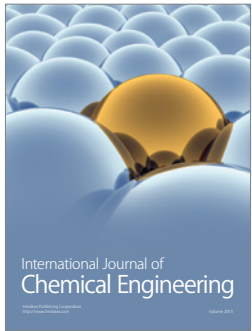


**International Journal of  
Distributed  
Sensor Networks**



**Hindawi**

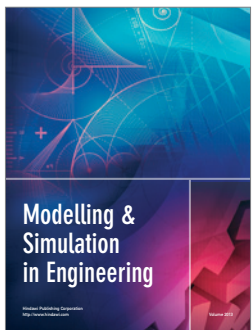
Submit your manuscripts at  
<http://www.hindawi.com>



**International Journal of  
Chemical Engineering**



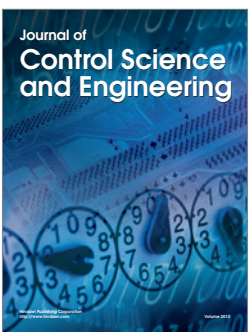
**VLSI Design**



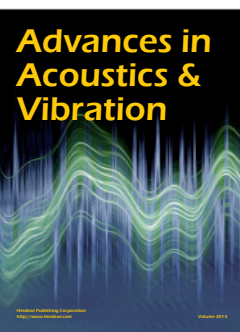
**Modelling &  
Simulation  
in Engineering**



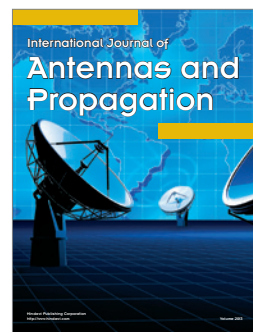
**Sensors**



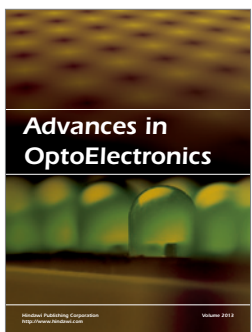
**Journal of  
Control Science  
and Engineering**



**Advances in  
Acoustics &  
Vibration**



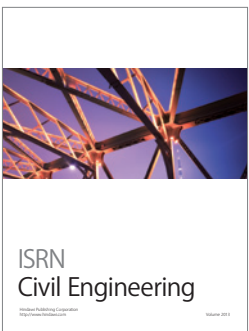
**International Journal of  
Antennas and  
Propagation**



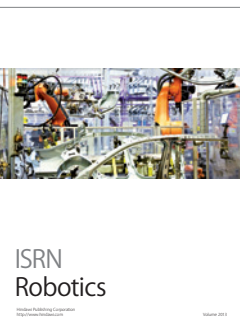
**Advances in  
OptoElectronics**



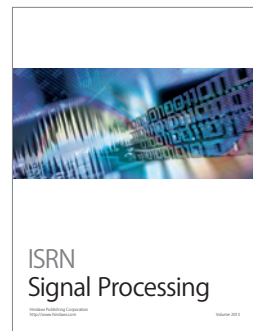
**ISRN  
Electronics**



**ISRN  
Civil Engineering**



**ISRN  
Robotics**



**ISRN  
Signal Processing**



**ISRN  
Sensor Networks**